THE JOURNAL OF PHYSICAL CHEMISTRY B

Article

pubs.acs.org/JPCB

Electron Transfer Reaction Dynamics of p-Nitroaniline in Water from Liquid to Supercritical Conditions

Koji Osawa,* Masahide Terazima, and Yoshifumi Kimura[†,‡]

Department of Chemistry, Graduate School of Science, Kyoto University, Kyoto 606-8502, Japan

Supporting Information

ABSTRACT: Photoexcitation dynamics of p-nitroaniline (pNA) have been investigated by femto-second transient absorption spectroscopy in water from liquid to supercritical conditions; along the isochoric line from the ambient condition to 664 K at 40.1 MPa and along the isothermal line from 40.1 to 36.1 MPa at 664 K. The rates of the back electron transfer reaction from the photoexcited charge transfer state to the electronic ground state was determined by the bleach recovery of the ground state absorption, and the successive vibrational relaxation in the electronic ground state was determined by the hot-band decay which was apparent at the red edge of the absorption. The variation of the back electron transfer rate was compared with the prediction based on the electron transfer theory including the Franck−Condon active vibrational modes. The results indicated that both the free energy change of the reaction and the change of the intramolecular vibrational reorganization energy cause the characteristic density (or temperature) dependence of the back electron transfer rate. The density dependence of the vibrational relaxation rate was compared with the collision frequency and the coordination number of the solvent molecule around the solute estimated by the molecular dynamics simulations. The density dependence of the coordination of a water oxygen atom to an amino hydrogen atom of pNA was found to be correlated with the density dependence of vibrational relaxation rate.

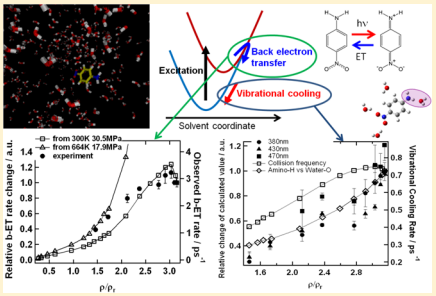

1. INTRODUCTION

Supercritical fluid with hydrogen bonding property such as supercritical water (SCW) and supercritical alcohols are interesting media in which characteristic reactions occur.[1] How their hydrogen bonding structure changes by the temperature and the pressure has been investigated extensively, with the use of various spectroscopic methods such as X-ray diffraction,[2] NMR,[3,4] Raman spectroscopy,[5] and so on. On the other hand, studies on the solute−solvent interaction in SCW and supercritical alcohols are still limited. In most studies, the change of solvation structure was detected by the temperature and pressure dependences of absorption or emission spectra. According to these studies, local density enhancement, which is a characteristic property of supercritical fluids,[6] was observed for the SCW and supercritical alcohols due to the solute−solvent attractive interaction and large density fluctuation. It is interesting how these changes of the solvation structure affect the basic chemical reactions such as electron transfer and proton transfer in SCW.[7−10] For example, Bartels's group have studied the dynamics of hydrated electron and hydroxyl radical in SCW by pulse radiolysis method, and reported unique density dependence of the rate constant for the reaction involving the hydrated electron. In cases of the bimolecular reactions related to the hydrated electron, both diffusion dynamics of electron and the change of the reaction free energy are involved in the reaction kinetics, and therefore the interpretation of the reaction mechanism became complicated.

In this paper, we present a study of the back electron transfer from the charge separated excited state of p-nitroaniline (pNA), and vibrational relaxation dynamics in the electronic ground state of pNA in SCW. pNA is a typical "push−pull" type solvatochromic molecule in which electron donor (amino group) and acceptor (nitro group) group are connected by a conjugated π-system. As shown in Scheme 1, pNA takes resonance structure between charge neutral (A) and charge separated (B) states. Oka et al. investigated spectral shift of pNA in SCW, and found that the absorption peak position shows monotonous blue shift with decreasing the solvent

Scheme 1. Neutral and Charge Transfer Molecular Structures of pNA

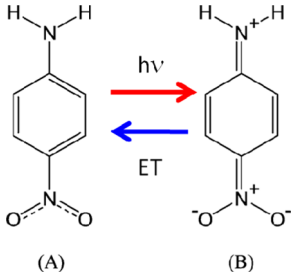

Received: June 18, 2012
Revised: August 20, 2012
Published: August 21, 2012

density along the isothermal line at 683 K.[11] The local density enhancement around the critical density was detected at very close to the critical temperature of water. Fujisawa et al. observed the NO_2 stretching mode of pNA in SCW over a wide density region, and found that the band shape is strongly dependent on the solvent temperature and density. By comparison with the DFT calculation results, they suggested that the dihedral angle of NH_2 to the aromatic plane is dependent on the solvent density. They also found that the NH_2 stretching mode in supercritical ethanol and methanol shows a large shift due to the changes of the hydrogen-bonding between pNA and solvent alcohols.[12]

The photoexcitation dynamics of pNA has been studied by using transient absorption spectroscopy (Scheme 2).[14−16] As

Scheme 2. Photoexcited Reaction Scheme of pNA

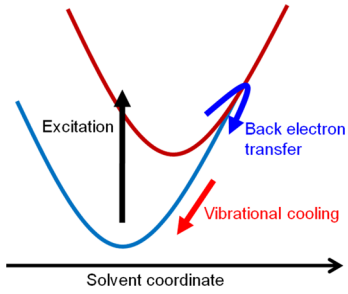

shown in Scheme 2, after the photoexcitation to the charge-separated excited state,[13] pNA mostly comes back to the electric ground state through the back electron transfer process in polar solvents to produce the vibrationally excited ground state molecule. Afterward, vibrationally excited pNA in the ground state is cooled down by the vibrational relaxation to the solvent molecules. Thomsen et al. measured the transient absorption spectrum of pNA in water and dioxane, and found that the quantum yield of intersystem crossing is very small in water (0.03).[14] Kovalenko et al. made more detailed measurements in various polar solvents including water.[15,16] They measured the transient absorption after the photoexcitation at 400 nm, and evaluated the back-electron transfer dynamics in subpicoseconds time scale by the bleach recovery dynamics in the blue-edge of the absorption spectrum. They also determined the vibrational cooling dynamics in the ground state in a few picosecond time scale by the hot band absorption decay dynamics in the red-edge of the absorption spectrum. They found that the vibrational relaxation in the ground state is accelerated by the solute−solvent hydrogen-bonding. It is quite an interesting issue how these dynamics are changed under the supercritical condition.

In the present work, we have investigated photoexcitation dynamics of pNA in water from ambient to supercritical conditions by the transient absorption spectroscopy, and discussed the experimental results with the aid of the spectral simulation and molecular dynamics simulation. In section 2, the experimental details will be presented. In section 3, we have evaluated the back electron transfer rate and the vibrational cooling rate from the time profiles of the transient absorption. In section 4, the back electron transfer rate will be compared with the prediction of the Marcus−Jortner theory and the vibrational cooling rate will be compared with the coordination number of the water molecules around pNA estimated by the MD simulations. The results indicate that the vibrational relaxation process and the back electron transfer process reflect different properties of SCW.

2. EXPERIMENTAL SECTION

2.1. Materials. pNA was purchased from Nacalai Tesque and recrystallized from ethanol before use. Distillated water was used as a solvent.

2.2. Transient Absorption Measurement. The transient absorption measurement was carried out using a portion of the output from an amplified Ti:sapphire laser system (Spectra Physics, Tsunami & Spitfire Pro XP, 800 nm, ca. 1.9 W, 120 fs, 1 kHz). We have used two different systems: one mainly for the measurement of the transient absorption spectrum (spectral system) and one for the time profile evaluation (time profile system). In the spectral system, a portion of the fundamental pulse was picked up to produce a white light continuum by focusing the pulse into a 3 mm CaF_2 crystal plate. The crystal was kept moving during measurement to avoid the damage by the laser pulse. The white continuum was separated into probe and reference pulses by a broadband beam splitter, and optical intensities of the probe pulse passing through the sample cell and the reference pulse were detected by a CCD camera equipped with a spectrometer (Princeton, Insight). The difference of the optical density (ΔOD) with and without pump pulse (400 nm, which was obtained by doubling the residual fundamental pulse) was measured by using the optical shutter, and the intensity fluctuation of probe pulses was corrected by the reference pulse measured simultaneously. The group velocity dispersion of probe pulse at each wavelength was corrected by measuring the optical Kerr response of pNA aqueous solution at each experimental condition. The system response was estimated to be ca. 350 fs.

In the time profile system, time profile of the transient absorption for the selected wavelength has been measured in the better signal-to-noise ratio than the spectral system.[17] Here a white continuum was generated by focusing the fundamental pulse into a 2 mm sapphire plate, and desirable wavelength (380, 430, or 470 nm) was extracted by a band pass filter. For the generation of 380 nm, the white continuum was frequency doubled by a 0.5 mm BBO crystal before the bandpass filter. The excitation pulse (400 nm) was generated by doubling a portion of the fundamental pulse as in the case of the spectral system. ΔOD at each delay time was evaluated by a toggle mode using an optical chopper, and the fluctuation of the probe pulse intensity was corrected by the reference pulse intensity.

For the measurement under supercritical conditions of water, a specially designed high-pressure and high-temperature cell was used as described elsewhere.[18] The optical path length was adjusted to be approximately 5 mm for the present measurement. The sample solution bubbled by argon gas was flowed into the high pressure cell at a rate of 0.8−1.0 mL min^{-1} using a high pressure syringe pump (ISCO, 260D), and controlled by the back-pressure regulator (JASCO, 880-81). The temperature of the system was controlled by a sheathed heater wounded around the cell and a thermocouple directly inserted into the sample chamber. The pressure of the system was regulated within ±0.1 MPa, and the fluctuation in temperature was mostly less than ±1 K.

The transient absorption spectra were measured along the 40.1 MPa isobar (between 297 and 664 K) and the 664 K isotherm (between 40.1 and 31.0 MPa). The critical temperature (T_C) and pressure (P_C) of water are 647 K and 22.1 MPa, respectively.[19] The densities at different temperatures and

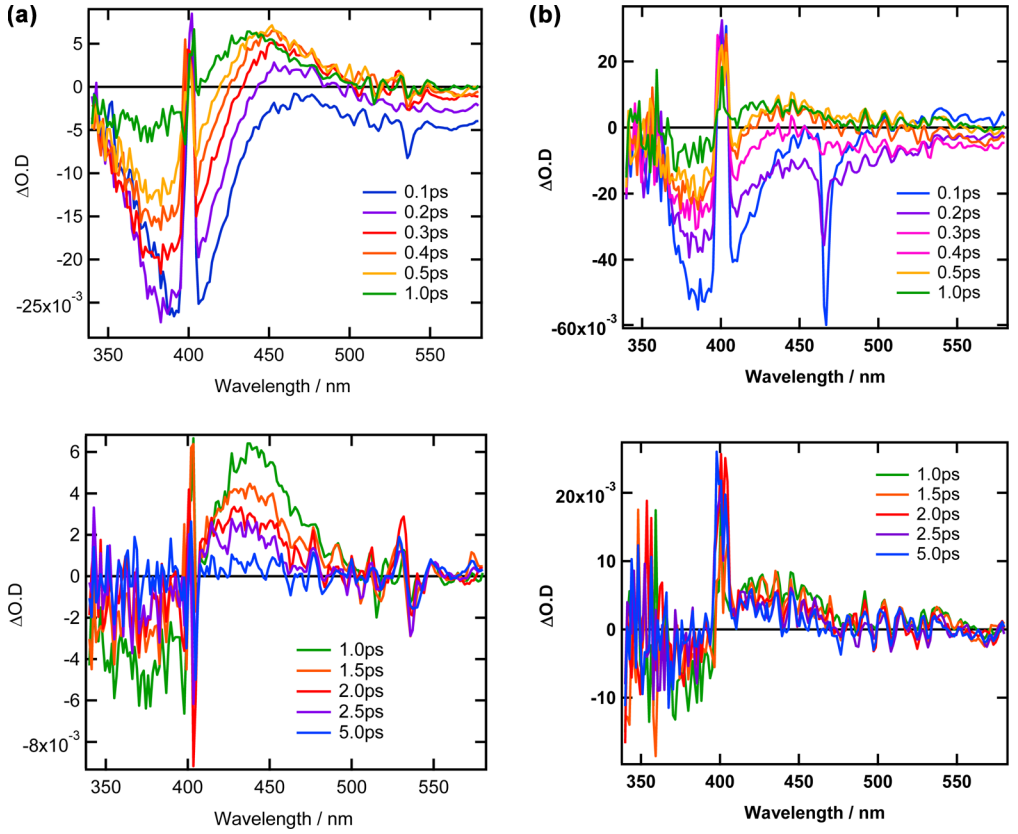

Figure 1. Transient absorption spectra of PNA in water at (a) 298 K and 40.1 MPa and (b) 664 K and 40.0 MPa. Upper figures show from 0.1 to 1.0 ps, and lower show from 1.0 to 5.0 ps.

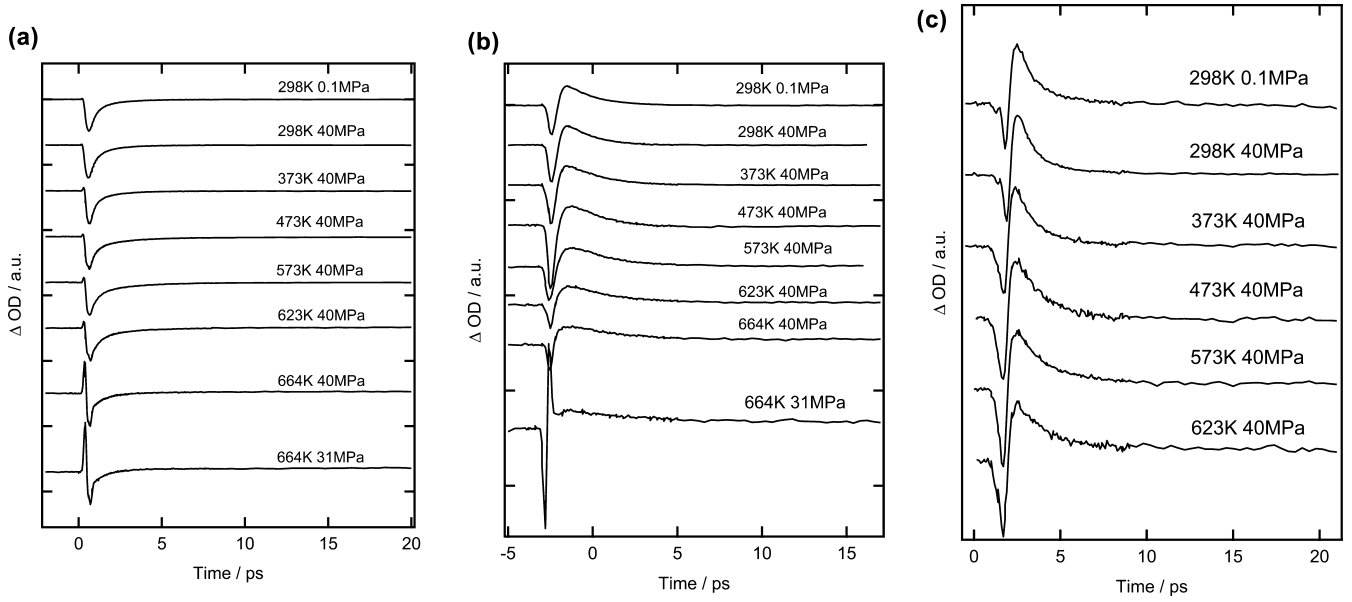

Figure 2. Time profiles of one color pump−probe measurement at various condition at (a) 380 nm, (b) 430 nm, and (c) 470 nm.

pressures were calculated by empirical equations of state.[19] The absorption peak maximum of the pNA shifted from 383 to 342 nm for the covering thermodynamic states under investigation (see Supporting Information, Figure S1).

2.3. Computational Method. Molecular dynamics simulations of pNA in water were performed using LAMMPS.[20] We employed the SPC/E model of water,[21] and OPLS/AA potential parameters for the intermolecular potential parameters between water and pNA.[22] Intramolecular geometry of pNA and water was fixed during the simulations. Simulations were performed using one pNA molecule and 492 water molecules by the NVT ensemble with the periodic boundary condition. The equations of motion were integrated by the velocity Verlet method, and the Nose thermostat was applied with the time constant of 0.1 ps. The Coulomb interaction was treated by the Ewald method, and the short-ranged interaction

dx.doi.org/10.1021/jp305970r | J. Phys. Chem. B 2012, 116, 11508−11516

was cut off at 9.0 Å. The time step was 1 fs, and after the initial 0.7 ns for the equilibration the solvation structure of water around pNA was analyzed by the data collected every 1 ps of the successive 2 ns.

3. RESULTS

Figure 1 shows the transient absorption spectra of pNA in water measured at (a) 298 K and (b) 664 K under 40.1 MPa. The spikelike signal at 400 nm is due to the scattering of the pump pulse, and that around 470 nm is due to the Raman signal of the sapphire cell window. In the earlier time within 1.0 ps, bleach recovery process was observed around 400 nm. After 1.0 ps, the bleach recovery had almost completed and the relaxation of the hot ground state was observed in the longer wavelength region around 430 nm. Even at the supercritical condition, no strong absorption appeared in the longer wavelength region than 450 nm, suggesting that the intersystem crossing to the triplet state is negligibly small.[23] However, due to the difficulty of the spectral measurement under high-pressure and high-temperature conditions, the spectral suffered from spikelike noises, and the signal-to-noise ratio (S/N) was not good. Therefore, in order to evaluate the time constants of the bleach recovery and the hot band decay, we decided to use the time profiles of some selected wavelengths measured by the time profile system, by which we can obtain signals with much better S/N. Although the single wavelength dynamics may not represent the exact time constant especially in the case of the hot-band dynamics, it will be possible to capture the density dependence by comparing the results obtained at different wavelengths.

Figure 2 shows time profiles of the transient absorption of pNA in water at various temperatures under 40.1 MPa at (a) 380 nm, (b) 430 nm, and (c) 470 nm. As is shown in Figure 2a (380 nm), the bleach recovery process showed more than two exponential kinetics, as reported previously. A sharp spike observed just around t = 0 ps is due to the optical response from the sapphire window of the high pressure cell. This spike became more evident as the temperature rises because the relative intensity of the signal to the spike decreases due to the lower concentration of pNA at the lower density. The time profile at 380 nm was fitted by a sum of four exponential decays convoluted with the system response function as

$$\Delta OD(t) = \int \mathrm{d}t' \sum_{i=1}^{4} a_i \exp\left(-\frac{t}{\tau_i}\right) I_{\mathrm{rf}}(t - t') \tag{1}$$

where a_i is the pre-exponential factor and τ_i is the time constant. $I_{\mathrm{rf}}(t)$ is the system response function determined by the OKE signal of acetonitrile, where the functional form of the response function was assumed to be

$$I_{\mathrm{rf}}(t) \propto \exp\left\{-\left(\frac{t - t_0}{\tau_s}\right)^2\right\} \tag{2}$$

Here τ_s is the instrumental response time. Since our response time was somewhat slow (ca. 0.30 ps), the time constant of the fastest component of kinetics was fixed to be 0.05 ps, which is taken from the result in ambient water according to ref 16. Since this process corresponds to the time constant of the intramolecular electron transfer with NO_2 twisting in the electronic excited state, the rate may not be strongly dependent on the solvent condition.[16] The time constant of the slowest component was fixed to 1000 ps (i.e., long enough), which corresponds to the decay of triplet states.[24] The second fastest component corresponds to the back electron transfer process, and the third component to the vibrational cooling process in the ground state assigned from the analysis of the transient absorption spectra in ref 16. In the evaluation of the time constants, we omit the time region of the spike from the fitting. Typical example of the fitting at 380 nm is shown in Figure 3, and the results of the fitting are summarized in Table 1.

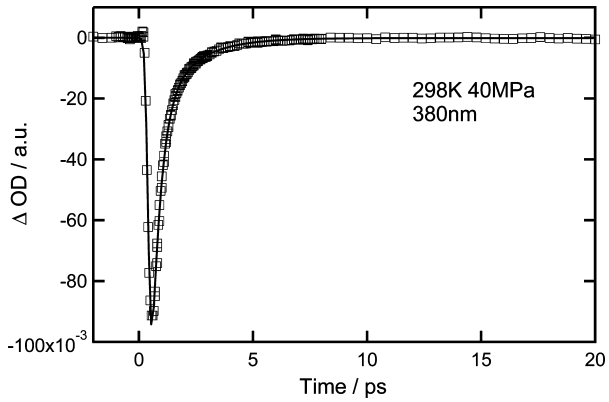

Figure 3. Fit of the time profiles of the measurement at 298 K and 40 MPa at 380 nm. The square represents experimental result, and the solid line represents the fit result.

Figures 2b and c shows the dynamics in the red-wavelength region of the ground state absorption (430 and 470 nm). Initially the signal showed the negative ΔOD mainly due to the ground state bleach and partially to the stimulated emission from the excited state. After the recovery of the bleach, the signal turned to be positive due to the hot band absorption, and decayed by the vibrational cooling. The time profiles of these transients were also simulated by the function of eq 1. Typical examples of the fitting are shown in Supporting Information (Figures S2(a) and (b) for the fitting at 430 nm and 470 nm) and the results of the fittings are summarized in Table 1.

4. DISCUSSION

4.1. Back Electron Transfer. As is shown in Table 1, the back electron transfer rate, k_{et}, once increases from 297 to 373 K and then decreases with increasing the temperature and decreasing the solvent density. The trend at the higher temperature than 373 K may be correlated with the decreasing polarity of water, which causes the reaction free energy change. In order to discuss the rate change with the thermodynamic states of water, we tried to evaluate the relative change of the back electron transfer rate based on the theory of Marcus and co-workers.[25] The electron transfer rate is given by

$$k_{\mathrm{et}} = \frac{2|V_{\mathrm{el}}|^2}{\hbar}\mathrm{Re}\int_0^\infty \mathrm{d}t \prod_i \langle 0_i|0_i(t)\rangle \exp[i\omega_{\mathrm{eg}}t - g(t)] \tag{3}$$

where V_{el} is electronic coupling between the ground and the excited states, and ω_{eg} is the energy difference between the excited and ground states minima. The function $\langle 0_i|0_i(t)\rangle$ represents the contribution of the intramolecular vibrations as

dx.doi.org/10.1021/jp305970r | J. Phys. Chem. B 2012, 116, 11508−11516

Table 1. Cooling Dynamics of pNA in Water under Several Pressure and Temperature Conditions[a]

T/K	P/MPa	ρ_r	λ/nm	a_3	a_4	τ_2/ps	τ_3/ps
298	40.1	3.15	380	−0.29 ± 0.01	0.00 ± 0.001	0.35 ± 0.02	1.38 ± 0.10
			430	0.30 ± 0.04	0.00 ± 0.001	0.33 ± 0.01	1.41 ± 0.03
			470				
298	0.1	3.10	380	−0.26 ± 0.02	0.00 ± 0.001	0.35 ± 0.01	1.45 ± 0.09
			430	0.23 ± 0.001	0.00 ± 0.02	0.31 ± 0.02	1.55 ± 0.01
			470				
373	40.1	3.03	380	−0.17 ± 0.002	−0.00 ± 0.001	0.31 ± 0.02	1.50 ± 0.14
			430	0.35 ± 0.01	0.00 ± 0.001	0.29 ± 0.02	1.89 ± 0.06
			470	2.47 ± 3.75	0.06 ± 0.016	0.40 ± 0.43	1.32 ± 0.20
423	40.1	2.91	380	−0.23 ± 0.04	−0.01 ± 0.002	0.32 ± 0.03	1.52 ± 0.22
			430	0.16 ± 0.01	0.00 ± 0.002	0.27 ± 0.01	2.10 ± 0.11
			470				
473	40.1	2.77	380	−0.25 ± 0.08	−0.02 ± 0.002	0.36 ± 0.02	2.28 ± 0.15
			430	0.20 ± 0.01	−0.01 ± 0.001	0.35 ± 0.01	1.83 ± 0.06
			470	0.91 ± 0.38	−0.02 ± 0.006	0.25 ± 0.20	1.81 ± 0.24
573	40.1	2.37	380	−0.29 ± 0.02	−0.01 ± 0.001	0.38 ± 0.01	2.33 ± 0.06
			430	0.34 ± 0.03	0.01 ± 0.001	0.46 ± 0.01	2.09 ± 0.06
			470	0.68 ± 0.15	0.05 ± 0.004	0.21 ± 0.06	1.73 ± 0.06
623	40.1	2.12	380	−0.27 ± 0.03	0.01 ± 0.004	0.44 ± 0.03	2.55 ± 0.29
			430	0.23 ± 0.01	0.02 ± 0.001	0.30 ± 0.01	2.64 ± 0.08
			470	1.20 ± 0.77	0.25 ± 0.44	0.39 ± 0.40	2.03 ± 0.50
673	40.1	1.72	380	−0.13 ± 40	0.05 ± 0.048	0.63 ± 0.03	3.15 ± 0.45
			430	0.09 ± 0.002	0.02 ± 0.001	0.19 ± 0.01	3.42 ± 0.16
			470				
673	31.0	1.46	380[b]			0.90 ± 0.05	4.96 ± 1.23
			430	0.03 ± 0.002	0.01 ± 0.01	0.19 ± 0.01	4.39 ± 0.60
			470				

[a] a_3, a_4 are relative values when a_2 is fixed to −1. a_1 is not shown because the values contain the contribution from the spike noise to some extent (see text). τ_1 and τ_4 are fixed to 0.05 and 1000 ps, respectively. [b] Since the artifact at $t = 0$ was significant large, only the slower part of the kinetics was determined.

$$\langle 0_i|0_i(t)\rangle = \exp\left(\frac{\Delta_i^2}{2}(2\bar{n}_i + 1)[\cos(\omega_i t) - 1] - i\frac{\Delta_i^2}{2}\sin(\omega_i t)\right) \quad (4)$$

where

$$\bar{n}_i = [\exp(\hbar\omega_i/kT) - 1]^{-1} \quad (5)$$

The value of ω_i represents the vibrational frequency of the ith vibrational mode and Δ_i is the dimentionless displacement between the excited state and the ground state minima along the vibrational coordinates. Intramolecular reorganization energy (λ_V) is given as a sum of $(1/2)\omega_i\Delta_i^2$ over all active vibrational modes. The absorption spectrum can be expressed in a similar manner as[25]

$$\mathrm{OD}(\omega) \propto \omega \mathrm{Re}\int_0^\infty \mathrm{d}t \prod_i \langle 0_i|0_i(t)\rangle \exp\left[i(\omega - \omega_{eg})t - g(t)\right] \quad (6)$$

For the Brownian oscillator model in the high temperature limit, the solvent line shape function is expressed by

$$g(t) = g_R(t) + ig_I(t) \quad (7)$$

where

$$g_R(t) = \frac{2\lambda_S kT}{\Lambda^2}[\exp(-\Lambda t/\hbar) + \Lambda t/\hbar - 1] \quad (8)$$

$$g_I(t) = \frac{\lambda_S}{\Lambda}[1 - \exp(-\Lambda t/\hbar)] \quad (9)$$

Here λ_S is the solvent reorganization energy and Λ is the modulation frequency of the solvent oscillator.

Unfortunately, the available information of the electronic state of pNA in supercritical water is quite limited. For example, no experimental data for the intramolecular vibrational displacement of pNA is available in water under ambient conditions, needless to say in water under supercritical condition. Further, the value of the reaction free energy is not available under supercritical conditions. Therefore, in this

paper, we made several simplified assumptions to estimate the density dependence of the back electron transfer rate.

First the solvent shifts of the reaction free energy and the solvent reorganization energy were estimated based on the following assumption. As was studied by Oka and Kajimoto, the solvatochromic shift of pNA was well described by the dielectric continuum model except for the spectrum very close to the critical point.[9] Therefore, we employ the basic idea from the dielectric continuum model. According to the dielectric continuum model,[26] $\Delta\omega_{eg}$ ($\equiv \omega_{eg} - \omega^0_{eg}$, where ω^0_{eg} denotes the reaction free energy in vapor) and λ_S can be expressed as follows:

$$\Delta\omega_{eg} = \frac{\mu_g^2 - \mu_e^2}{4\pi\varepsilon_0 a^3}\frac{n^2 - 1}{2n^2 + 1} + \frac{\mu_g^2 - \mu_e^2}{4\pi\varepsilon_0 a^3}L(\varepsilon, n) \quad (10)$$

$$\lambda_S = \frac{\left(\mu_g^2 - \mu_e^2\right)^2}{4\pi\varepsilon_0 a^3}L(\varepsilon, n) \quad (11)$$

$$L(\varepsilon, n) = \frac{\varepsilon - 1}{\varepsilon + 2} - \frac{n^2 - 1}{n^2 + 2} \quad (12)$$

where μ_g and μ_e are the dipole moments of the ground and excited states. By neglecting the first term of eq 10, we get following linear relationship between λ_S and ω_{eg} as

$$\Delta\omega_{eg} = -\frac{\mu_e/\mu_g + 1}{\mu_e/\mu_g - 1}\lambda_S \quad (13)$$

On the other hand, if the intramolecular reorganization energy (λ_V) is independent of the solvent condition, the absorption peak ν_{abs} is given by the following equation

$$\nu_{abs} = \nu_0 - \Delta\omega_{eg} + \lambda_S \quad (14)$$

where ν_0 is the absorption peak without solvent. If the linear relationship of eq 13 holds, the absorption peak shift is regarded as the linear function of the free energy change or the solvent reorganization energy. Under these assumptions, we estimated the solvent reorganization energy and the reaction free energy. In the calculation, the dipole moments of the ground state ($\mu_g = 6D$) and the excited state ($\mu_e = 14D$) were taken from literature.[27] The value of ν_0 was estimated by the extrapolation of the plot of $\Delta\nu_{abs}$ against $L(\varepsilon, n)$ to $L(\varepsilon, n) = 0$ (see the Supporting Information, Figure S3). As is clearly shown in Figure S3, the dielectric continuum model breaks down at the high density. However, we consider that the proportionality between λ_S and ω_{eg} may hold under such condition.[28] Estimated λ_S against the reduced density is shown in Figure 4. λ_S increases monotonically with increasing the density, although at the very high density region the value turns to decrease with increasing the solvent density.

In order to estimate the intramolecular reorganization energy, we tried to make a fitting of absorption spectrum with the modification of the intramolecular reorganization energy of pNA determined for the methanol solution. Moran and Kelley measured the resonance Raman spectra and their excitation profiles of pNA in various solvent.[29] We employed the parameters determined for methanol, since the resonance Raman spectrum of pNA in water is not so different from that in methanol at 355 nm excitation. In order to simulate the spectrum in water, we rescaled the parameters of methanol. The results of the fit at the thermodynamic states of the highest and the lowest densities (298 K and 30.5 MPa (a) and 664 K and 17.9 MPa (b)) are shown in Figure 5. It was found that both spectra could not be simulated by a single set of intramolecular reorganization parameters. In order to simulate the spectrum, all the displacements Δ_i were multiplied by 1.1 in (a) and 1.4 in (b) (estimated ω^0_{eg} was 27 968 cm^{-1} in (a) and 28 119 cm^{-1} in (b)). This means that the assumption that the intramolecular reorganization energy is independent of the solvent condition is not necessarily correct. The origin of the discrepancy will be discussed later. The density dependence of the reaction free energy estimated from eq 13 in (a) and (b) is shown in Figure 6. Here we will discuss these two extreme cases at the highest and the lowest densities in the measurement.

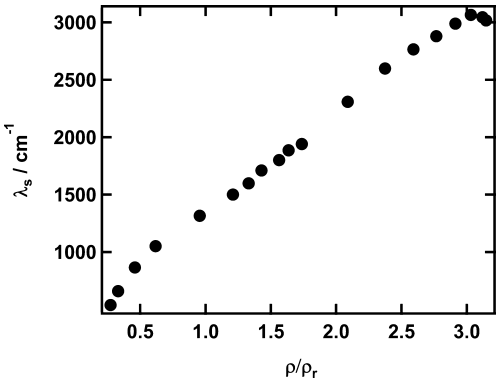

Figure 4. Plot of the solvent reorganization energy estimated from the observed absorption spectrum peak shift against the reduced density.

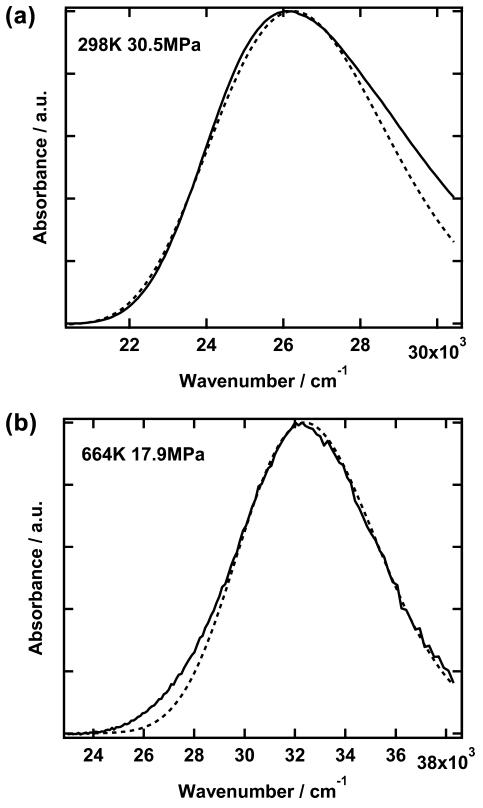

Figure 5. Absorption spectra of pNA in water (a) at 298 K under 30.5 MPa and (b) at 664 K under 17.9 MPa (solid curves), and theoretically calculated spectra (dashed curves).

dx.doi.org/10.1021/jp305970r | J. Phys. Chem. B 2012, 116, 11508−11516

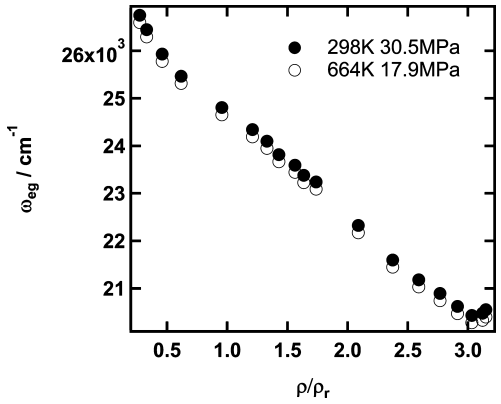

Figure 6. Plot of the reaction free energy estimated from eq 13 at 298 K under 30.5 MPa (●) and at 664 K under 17.9 MPa (○).

Figure 7 shows the relative change of the back electron transfer rate by using the parameters for (a) and (b),

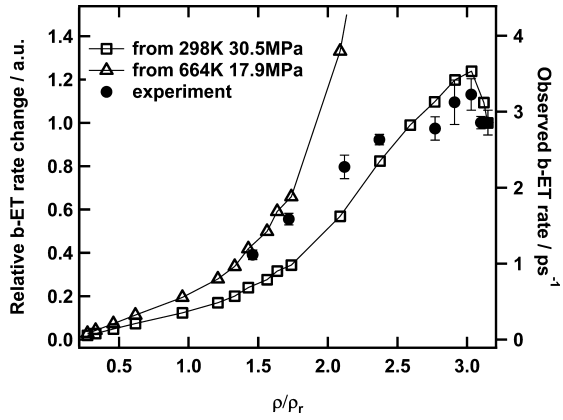

Figure 7. Plot of the relative change of the calculated back electron transfer rate from the parameters of (a) at 298 K under 30.5 MPa (□) and (b) at 664 K under 17.9 MPa (△) with the observed rate (●) against the reduced density. The calculation was scaled to the value at 298 K under 30.5 MPa from (a).

respectively. Since we do not have enough information for V_{el} and its density dependence, we simply assumed that it does not change by density, and compared its relative change with the experiment. In the figure, the calculation is scaled to the value obtained from (a) at 300 K and 30.5 MPa. The relative change of the calculation from (a) reproduced the experimental result qualitatively, especially the maximum peak at 373 K (ρ_r = 3.03). According to the calculation, the increase of the rate from ambient condition to ρ_r = 3.03 is due to the decreasing of the reaction free energy reflecting the red-shift of the absorption of pNA with increasing the temperature at this region (Figure 6). We are not sure of the origin of the red shift with increasing the temperature at present.

At the lower density region, the relative change of the observed back electron transfer rate deviates from the calculation using the parameters of (a), and the behavior approaches that of the calculation of (b). This indicates that the density dependence of the intramolecular vibrational reorganization energy affects the back electron transfer rate change. When λ_v increases, the back electron transfer process through the vibrational excited state is accelerated, and vibrational reorganization energy λ_v at (b) (4952.77 cm^{-1}) is higher than that at (a) (3233.51 cm^{-1}) by 1719 cm^{-1}. Due to the increase of the intramolecular reorganization energy, the reaction free energy is also estimated to be smaller for the case (b). Therefore, in the low density region, the back electron transfer rate becomes higher than the prediction from the calculation of (a).

Considering the rough estimation of the parameters, the coincidence is surprising. In this model, the values of Δ_i of methanol are employed and assumed to change by the same scale for all the vibrational modes. However, Δ_i for each mode is expected to change uniquely by the density.[27] Further, and more importantly, at the elevated temperature, the lower frequency vibrational mode, which was not taken into account in our calculation, becomes thermally active and the transition from higher quanta may contribute to the Franck−Condon transition. Including the contribution of lower frequency mode to the calculation is expected to accelerate the back electron transfer process. To simulate complete density dependence of the back electron transfer rate change, it is necessary to determine intramolecular vibrational parameters at each density with consideration of these effects.

4.2. Vibrational Relaxation. Figure 8 shows the solvent density dependence of the vibrational cooling rates determined

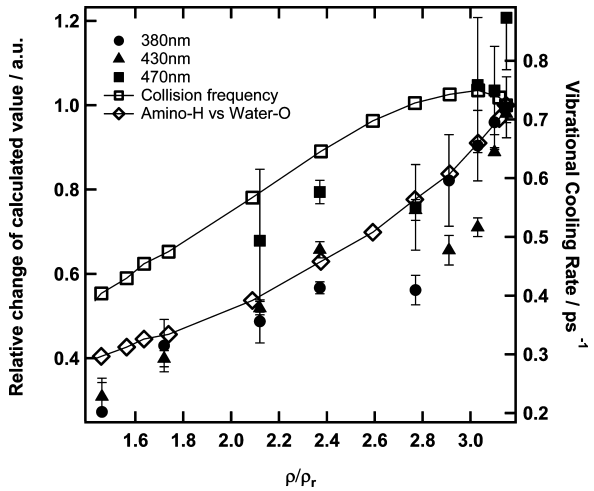

Figure 8. Plot of the observed vibrational relaxation rate at 380 nm (●), at 430 nm (▲), and at 470 nm (■) with the relative change of the collision frequency evaluated from local density of water oxygen atoms around the pNA center (□) and the coordination number of water oxygen atoms to amino hydrogen atoms of pNA (◇) estimated from the MD simulation.

by different probe wavelengths. The density dependences observed at 380 and 430 nm were close to each other. Although the rates determined at 470 nm are slightly different at the lower density region, we suspected that a minor contribution of the intersystem crossing to the triplet state may be involved in the signal response at 470 nm. We consider the hot band decay is the main contribution to the signal at 430 and 380 nm.

The isolated binary collision model is the simplest way to interpret the vibrational cooling rate, where the collision number between the solvent and solute dominates the density dependence of the vibrational cooling rate.[30] On the other hand, for pNA, it has been reported that the hydrogen-bonding between pNA and water is important for the vibrational cooling.[12] To understand the origin of the density dependence of vibrational relaxation rate, we compared the rate with the

dx.doi.org/10.1021/jp305970r | J. Phys. Chem. B 2012, 116, 11508−11516

collision frequency and the hydrogen-bond obtained from the MD simulation. Collisional frequency between pNA and water molecule (Z) was estimated by the following equation

$$Z = n_{\mathrm{local}}\left(\frac{4\pi r_{\mathrm{local}}{}^3}{3}\right)^{-1}\langle u\rangle,$$

$$n_{\mathrm{local}} = \rho 4\pi \int_0^{r_{\mathrm{local}}} g(r) r^2\, \mathrm{d}r,$$

$$\langle u\rangle = \left(\frac{8k_{\mathrm{B}}T}{\pi m}\right)^{1/2} \qquad (15)$$

where n_{local} represents the coordination number of water molecule around pNA, ρ represents the density of solvent, and $\langle u\rangle$ is the average velocity of the water molecules. r_{local} stands for the radius of the local sphere region around pNA, and $g(r)$ is the radial distribution function (RDF) between the centers of pNA and water molecules. Figure 9a shows the RDF between the pNA center (center of benzene ring) and an oxygen atom of water molecule. Here we estimated the coordination number n_{local} by integration of the radial distribution function within 5.5 Å. White squares in Figure 8 show the density dependence of the collision frequency change calculated by (15) using obtained n_{local}. In the figure, the collision frequency is scaled to the value of the vibrational cooling rate at 380 nm at ρ_{r} = 3.15. This figure shows that the change of the collision frequency does not correlate with the rate change, especially at the higher density (or lower temperature) region.

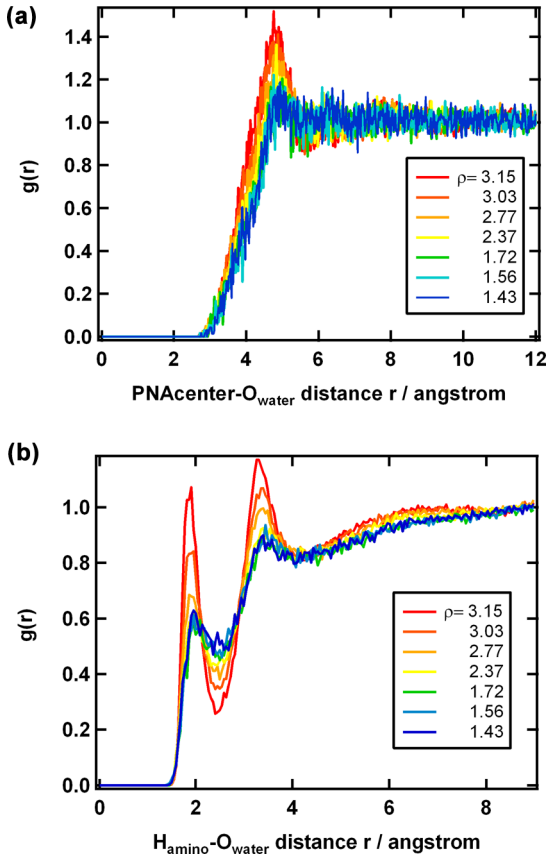

Figure 9. Radial distribution function between (a) the pNA center and water oxygen atom and (b) the amino hydrogen atom of pNA and the water oxygen atom.

On the other hand, in supercritical methanol or ethanol, the solute−solvent hydrogen-bonding shows a large change with the solvent density according to Raman study.[12] The study of the solute−solvent hydrogen-bonding between p-aminobenzonitrile and water molecules also indicated the large density dependence of the hydrogen-bonding at a corresponding density region.[31] Furthermore, it was previously found that the vibrational relaxation is accelerated by the hydrogen bonding for a dye molecule,[32] and also for pNA.[15,16] Therefore, we compared the reaction rates with the number of hydrogen-bonds between water and the amino group of pNA. Figure 9b shows the radial distribution function between hydrogen atoms of amino group of pNA and oxygen atoms of water molecules. By integrating RDF within 2.4 Å, the number of water O atoms which are hydrogen-bonded to amino H atoms can be estimated. The estimated number of hydrogen-bonds is compared the vibrational cooling rate in Figure 7 (white diamond). In the figure, the number of the hydrogen-bonding is scaled to the value of the vibrational cooling rate at 380 nm at ρ_{r} = 3.15. It shows a good correlation between the vibrational relaxation rate and the number of hydrogen bond to amino H atoms. Especially both change drastically in high density region. As mentioned in the Introduction, Kovalenko et al. reported vibrational relaxation is accelerated by solute−solvent hydrogen bonding,[15] and Fujisawa reported that NH_2 stretching mode frequency shift of pNA by density in supercritical ethanol and methanol reflect on solute−solvent hydrogen bonding, which other modes do not.[12] Taking these studies and this experimental result into consideration, it is plausible that hydrogen bond of water to pNA amino group plays an important role on vibrational relaxation process.

5. CONCLUSION

In this Article, photoexcitation dynamics of pNA have been studied by the transient absorption spectroscopy from the liquid to the supercritical water. The back electron transfer rate from the charge transfer excited state to the electronic ground state was compared to the estimation based on the theory of Marcus and Jortner using the parameters obtained from the fitting of steady state absorption spectra, and the relative change of experimental result could be roughly reproduced. The density (or temperature) dependence of the electron transfer rate was qualitatively reproduced by the Marcus−Jortner theory, indicating the dielectric property of water is important for the electron transfer process. The deviation of the calculation from the experimental result is possibly due to the density dependence of the intramolecular vibrational energy, especially for the low frequency modes of pNA and the contribution of the electric coupling neglected in the evaluation. The density dependence of the vibrational relaxation rate in the electronic ground state was compared with the local solvation structure evaluated by the molecular dynamics simulation. The vibrational relaxation rate was found to be not correlated with the simple collision frequency between pNA and water molecules, rather correlated with the amount of hydrogen bonding coordination of water molecules to the pNA amino group. This result suggests the local hydrogen bonds between amino group of pNA and water molecules promoting the vibrational relaxation process. A more sophisticated theoretical treatment considering both electric structure of solute and solvent effect[33] is required for precise

dx.doi.org/10.1021/jp305970r | J. Phys. Chem. B 2012, 116, 11508−11516

evaluation of the correlation between back electron transfer rate and solvent or intramolecular vibrational reorganization energy. From an experimental side, it is important to study the correlation between the relaxation dynamics of the excited intramolecular vibrational modes[34,35] and the vibrational relaxation process of pNA molecule in SCW to investigate specific solute−solvent interaction on the process.

■ ASSOCIATED CONTENT

Supporting Information

Absorption spectra of pNA in water at various temperatures and pressures, the fitting results of the time profiles at 430 and 470 nm, and the plot of the absorption peak against the reaction field. This material is available free of charge via the Internet at http://pubs.acs.org.

■ AUTHOR INFORMATION

Corresponding Author

*E-mail: osawa@kuchem.kyoto-u.ac.jp. Tel: 075-753-4024.

Present Address

[†]Department of Chemical Science and Technology, Faculty of Bioscience and Applied Chemistry, Hosei University.

Notes

The authors declare no competing financial interest.

[‡]E-mail: ykimura@hosei.ac.jp.

■ ACKNOWLEDGMENTS

This work is supported by the fund from Japan Society for Promotion of Science (JSPS) (No. 19350010). K.O. acknowledges to the support from the Research Fellowship of JSPS for Young Scientists. K.O. was supported by the research fellowship of Global COE program, International Center for Integrated Research and Advanced Education in Material Science, Kyoto University, Japan.

■ REFERENCES

(1) Savage, P. E. *Chem. Rev.* **1999**, *99*, 603−622.

(2) Yamanaka, K.; Yamaguchi, T.; Wakita, H. *J. Chem. Phys.* **1994**, *101*, 9830−9836.

(3) (a) Matubayasi, N.; Wakai, C.; Nakahara, M. *J. Chem. Phys.* **1997**, *107*, 9133−9140; **1999**, *110*, 8000−8011. (b) Matubayasi, N.; Nakao, N.; Nakahara, M. *J. Chem. Phys.* **2001**, *114*, 4107−4115.

(4) (a) Hoffmann, M. M.; Conradi, M. S. *J. Am. Chem. Soc.* **1997**, *119*, 3811−3817. (b) Hoffmann, M. M.; Conradi, M. S. *J. Phys. Chem. B* **1998**, *102*, 263−271.

(5) Ikushima, Y.; Hatakeda, K.; Saito, N.; Arai, M. *J. Chem. Phys.* **1998**, *108*, 5855−5860.

(6) (a) Bennett, G. E.; Johnston, K. P. *J. Phys. Chem.* **1994**, *98*, 441−447. (b) Niemeyer, E. D.; Dunbar, R. A.; Bright, F. V. *Appl. Spectrosc.* **1997**, *51*, 1547−1553. (c) Minami, K.; Mizuta, M.; Suzuki, M.; Aizawa, T.; Arai, K. *Phys. Chem. Chem. Phys.* **2006**, *8*, 2257−2264. (d) Kometani, N.; Takemiya, K.; Yonezawa, Y.; Amita, F.; Kajimoto, O. *Chem. Phys. Lett.* **2004**, *394*, 85−89. (e) Osada, M.; Toyoshima, K.; Mizutani, T.; Minami, K.; Watanabe, M.; Adschiri, T.; Arai, K. *J. Chem. Phys.* **2003**, *118*, 4573−4577. (f) Mikami, K.; Ohashi, T.; Suzuki, M.; Aizawa, T.; Adshjiri, T.; Arai, T. *Anal. Sci.* **2006**, *22*, 1417−1423.

(7) (a) Lin, M.; Katsumura, Y.; Muroya, Y.; He, H.; Wu, G.; Han, Z.; Miyazaki, T.; Kudo, H. *J. Phys. Chem. A* **2004**, *108*, 8287−8295. (b) Muroya, Y.; Lin, M.; De Waele, V.; Hatano, Y.; Katsumura, Y.; Mostafavi, M. *J. Phys. Chem. Lett.* **2010**, *1*, 331−335.

(8) (a) Cline, J.; Takahashi, K.; Marin, T. W.; Jonah, C. D.; Bartels, D. M. *J. Phys. Chem. A* **2002**, *106*, 12260−12269. (b) Marin, T. W.; Cline, J. A.; Takahashi, K.; Bartels, D. M.; Jonah, C. D. *J. Phys. Chem. A* **2002**, *106*, 12270−12279. (c) Bartels, D. M.; Takahashi, K.; Cline, J. A.; Marin, T. W.; Jonah, C. D. *J. Phys. Chem. A* **2005**, *109*, 1299−1307. (d) Martin, T. W.; Takahashi, K.; Jonah, C. D.; Chemerisov, S. D.; Bartels, D. M. *J. Phys. Chem. A* **2007**, *111*, 11540−11551.

(9) (a) Green, S.; Xiang, T.; Johnston, K. P.; Fox, M. A. *J. Phys. Chem.* **1995**, *99*, 13787−13795. (b) Ryan, E. T.; Xiang, T.; Johnston, K. P.; Fox, M. A. *J. Phys. Chem.* **1996**, *100*, 9395−9402.

(10) (a) Kobayashi, I.; Terazima, M.; Kimura, Y. *J. Phys. Chem. B* **2012**, *116*, 1043−1052. (b) Kobayashi, I.; Terazima, M.; Kimura, Y. *J. Phys. Chem. B* **2012**, *116*, 7604−7604.

(11) Oka, H.; Kajimoto, O. *Phys. Chem. Chem. Phys.* **2003**, *5*, 2535−2540.

(12) Fujisawa, T.; Terazima, M.; Kimura, Y. *J. Phys. Chem. A* **2008**, *22*, 5515−5526.

(13) Sinha, H. K.; Yates, K. *Can. J. Chem.* **1990**, *69*, 550−557.

(14) Thomsen, C. L.; Thøgersen, J.; Keiding, S. R. *J. Phys. Chem. A* **1998**, *102* (7), 1062−1067.

(15) Kovalenko, S. A.; Shcanz, R.; Farztdinov, V. M.; Hennig, H.; Ernsting, N. P. *Chem. Phys. Lett.* **2000**, *323*, 312−322.

(16) Kovalenko, S. A.; Shcanz, R.; Hennig, H.; Ernsting, N. P. *J. Chem. Phys.* **2001**, *115*, 3256−3273.

(17) Nishiyama, Y.; Terazima, M.; Kimura, Y. *Chem. Phys. Lett.* **2010**, *491*, 164−168.

(18) (a) Fujisawa, T.; Maru, E.; Amita, F.; Harada, M.; Uruga, T.; Kimura, Y. In *Water, Steam, and Aqueous Solutions for Electric Power*; Proceedings of the 14th International Conference on the Properties of Water and Steam, Kyoto, Japan, 2004; p 445. (b) Kimura, Y.; Amita, F.; Fujisawa, T. *Rev. High Pressure Sci. Technol.* **2006**, *16*, 87−94.

(19) Wagner, W.; Kruse, A. *Properties of water and steam*; Springer-Verlag: Berlin, 1998.

(20) Plimpton, S. J. *J. Comput. Phys.* **1995**, *117*, 1−19, http://lammps.sandia.gov.

(21) Berendsen, H. J. C.; Gregera, J. R.; Straatsma, T. P. *J. Phys. Chem.* **1987**, *91*, 6269−6271.

(22) (a) Rizzo, R. C.; Jorgensen, W. L. *J. Am. Chem. Soc.* **1999**, *121*, 4827−4836. (b) Price, M. L. P.; Ostrovsky, D.; Jorgensen, W. L. *J. Comput. Chem.* **2001**, *22*, 1340−1352.

(23) Wolleben, J.; Testa, A. C. *J. Phys. Chem.* **1977**, *81*, 429−431.

(24) Thomsen, C. L.; Thøgersen, J.; Keiding, S. R. *J. Phys. Chem. A* **1998**, *102*, 1062−1067.

(25) (a) Marcus, R. A.; Sutin, N. *Biochim. Biophys. Acta* **1985**, *811*, 265−322. (b) Marcus, R. A. *J. Phys. Chem.* **1989**, *93*, 3078−3086.

(26) McRae, E. G. *J. Phys. Chem.* **1957**, *61*, 562−572.

(27) Liptay, W. In *Excited States*; Lim, E. C., Ed.; Wiley: New York, 1974; Vol. *1*, p 129.

(28) Kimura, Y.; Takebayashi, Y.; Hirota, N. *J. Chem. Phys.* **1998**, *8*, 1485−1498.

(29) Moran, A. M.; Kelley, A. M. *J. Chem. Phys.* **2001**, *115*, 912−924.

(30) Olschewski, M.; Knop, S.; Lindler, J.; Vöhringer, P. *J. Chem. Phys.* **2011**, *134*, 214504.

(31) Osawa, K.; Hamamoto, T.; Fujisawa, T.; Terazima, M.; Sato, H.; Kimura, Y. *J. Phys. Chem. A* **2009**, *113*, 3143−3154.

(32) Terazima, M *Chem. Phys. Lett.* **1999**, *305*, 189−196.

(33) Yokogawa, D.; Sato, H.; Sakaki, S.; Kimura, Y. *J. Phys. Chem. B* **2010**, *114*, 910−914.

(34) Kozich, V.; Werncke, W.; Dreyer, J.; Brzezinka, K. -W.; Rini, M.; Kummorow, A.; Elsaesser, T. *J. Chem. Phys.* **2002**, *117*, 719−726.

(35) Kozich, V.; Werncke, W.; Vodchits, A. I.; Dreyer, J. *J. Chem. Phys.* **2003**, *118*, 1808−1814.